F.Özil[1], S.Demirtas[2], H.Doğan[3], H.Öztürk[4], M.Sabuncu[4]

DYNAMIC STABILITY OF DIAMOND FRAME STRUCTURES

[1]BMC Otomotiv Sanayi ve Ticaret A.Ş., Kemalpaşa St. No:288 Pınarbaşı, Izmir, Türkiye; e-mail: fundaozil.90@gmail.com.tr
[2]Erzincan Binali Yıldırım University, Department of Mechanical Engineering, Erzincan, Türkiye; e-mail: sdemirtas@erzincan.edu.tr
[3]Dokuz Eylül University Department of Electrical and Electronics Engineering, Tınaztepe Campus, Buca, İzmir, Türkiye; e-mail: hatice.dogan@deu.edu.tr
[4]Dokuz Eylül University Department of Mechanical Engineering, Tınaztepe Campus, Buca, İzmir, Türkiye; e-mail: hasan.ozturk@deu.edu.tr

Abstract. The in-plane dynamic and static stability of diamond beam structures under the periodic load is investigated. The diamond shape structure is assumed to be an Euler beam and modeled by using the Finite Element Method. The Bolotin approach is used for finding the dynamic instability regions. The natural frequencies and buckling load obtained from the generated finite element code are compared with ANSYS program results. Moreover, the effects of various boundary conditions, inclination angles, beam lengths, a beam having a tapered cross-section, and static/dynamic load parameters on unstable regions are investigated.

Key words*:* diamond-shaped frame, dynamic stability, finite element, static and dynamic loads.

1.Introduction.

Frames are used in engineering in structural configurations such as bridges, industrial structures, and skyscrapers. Also, the frame structures are widely used in the turbine, automotive, and machine industries. These frames are subjected to static and dynamic loads that may cause static and dynamic instability during operating conditions. Therefore, there are many researches on the static stability (buckling) and dynamic stability of frame structures. According to Bolotin's (1964) definition, the dynamic stability of mechanical systems represents the specific stability of motion. When this definition is examined, it is seen that three stages are included in the dynamic stability equation. These three stages are vibration analysis, static stability (buckling) analysis, and dynamic stability analysis. The bending of a Bernoulli-Euler beam has been developed using a modified couple stress theory by Park and Gao (2006). A variational formulation based on the principle of minimum total potential energy is employed in this study. Falsone and Settineri (2011) have studied a new finite element approach for the solution of the Timoshenko beam. They have used the finite element method similar to the Bernoulli-Euler beam theory. But it was considered a single fourth-order differential equation that governs the equilibrium of the Timoshenko beam. Briseghella et al. (1998) have used the finite element method to find the regions of the dynamic stability of beams and frames. Girgin et al. (2006) have developed a simplified procedure for determining approximate values for the buckling loads of both regular and irregular frames, where the procedure utilizes lateral load analysis of frames.

Zaslavsky (1981) has examined the elastic stability of portal frames consisting of hinged and/or fixed columns and hinged girder (beam) with an overhang under the action of a moving load. Thomas and Belek (1977) have studied the free-vibration characteristics of shrouded blade packets by using the finite element method. The effects of various weight ratios, flexural rigidity ratios, and length ratios between the blades and shrouds on the frequencies of vibration of the blade packet have been investigated.

Lin and Ro (2003) have developed a hybrid analytical/numerical method that permits the efficient dynamic analysis of planar serial-frame structures. The method has utilized a numerical implementation of a transfer matrix solution to the equation of motion. The semi-rigid connections between members of frame structures have been idealized as rotational and linear springs and the physical model representing each individual member has been assumed to consist of a flexible beam with springs and dashpots attached at both ends by Kawashima (1984). In-plane stability analysis of non-uniform cross-sectioned thin curved beams under uniformly distributed dynamic loads was investigated by using the Finite Element Method by Öztürk et al. (2006). Karaağaç et al. (2011) have studied the effects of a single-edge crack and its locations on the buckling loads, natural frequencies and dynamic stability of circular curved beams by using the Finite Element Method.

Öztürk and Sabuncu (2005) have examined the static and dynamic stabilities of a laminated composite cantilever beam having a linear translation spring and torsional spring as elastic supports subjected to periodic axial loading. Öztürk et al. (2015) have investigated the effect of crack depth and crack location on the in-plane static and dynamic stability of cracked multi-by frame structures subjected to periodic loading by using the Finite Element Method. Ibrahim et al. (2012) have studied the effects of crack depth and crack location on the in-plane free vibration of cracked frame structures by using the Finite element Method. The equation of motion in the matrix form of a tapered cantilever Bernoulli-Euler beam subjected to a follower force at the free end has been formulated by Lee based (1995) on the Lagrangian approach and the assumed mode method.

Covill et al. (2014) have examined the analysis of the diamond-shaped bicycles frames by using the Finite Element Method. The non-linear solutions for the large deflections of diamond-shaped frames have been derived by Jenkins et al. (1996). In this study, the frames have been loaded by forces applied at a pair of opposite joints, which are either pin-jointed or rigid. The experimental results obtained on square steel frames are compared with the nonlinear (exact) solutions and also with small deflection nonlinear and linear analyses.

In this study, a finite element model is developed for diamond-shaped frame structures. The Bernoulli-Euler beam theory is used in modeling the diamond frame structures. Natural frequencies and buckling load are calculated. Bolotin's approach is used for finding the dynamic instability regions. Matlab software is used for numerical analysis and calculated results are compared with ANSYS program results.

As can be seen from existing literature, any studies on the static and dynamic stability of diamond-shaped frame structures are not available. This study will make up for this deficiency.

2. Material and Method.

2.1. Finite Element Formulation. The problem addressed in this study is a diamond-shaped steel frame forming four beams with an inclination angle θ, shown in Fig. 1.

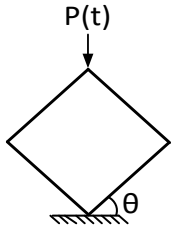

Fig. 1. Diamond-shaped frame.

The finite element method is used for modeling the frame. The beam element has two nodes with three degrees of freedom at each node and it is shown in Fig. 2.

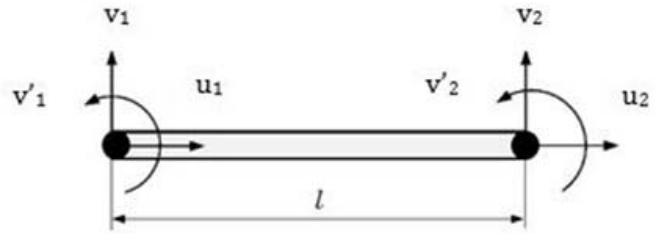

Fig. 2. Two nodes with six degrees of freedom beam element.

2.1.1. Mass and Stiffness Matrix. Mass and stiffness matrices for longitudinal and transverse vibrations of the uniform beam can be found in any finite element textbook and given below:

For transverse vibration,

$$\left[m^b\right]=\frac{\rho Al}{420}\begin{bmatrix}156 & 22l & 54 & -13l\\ 22l & 4l^2 & 13l & -3l^2\\ 54 & 13l & 156 & -22l\\ -13l & -3l^2 & -22l & 4l^2\end{bmatrix};\quad \left[k^b\right]=\frac{EI}{l^3}\begin{bmatrix}12 & 6l & -12 & 6l\\ 6l & 4l^2 & -6l & 2l^2\\ -12 & -6l & 12 & -6l\\ 6l & 2l^2 & -6l & 4l^2\end{bmatrix}. \tag{1}$$

For longitudinal vibration,

$$\left[\mathrm{m}^a\right]=\frac{\rho Al}{6}\begin{bmatrix}2 & 1\\ 1 & 2\end{bmatrix};\quad \left[\mathrm{k}^a\right]=\frac{EA}{l}\begin{bmatrix}1 & -1\\ -1 & 1\end{bmatrix}, \tag{2}$$

where ρ, E, I, A and l are mass density, elastic modulus, area moment of inertia, cross-section area and beam length, respectively.

The element mass and stiffness matrices, shown in Equations (1), (2), are superposed with the element matrices associated with the two-node element and given in

Equation (3):

$$\left[m_e\right]=\begin{bmatrix}m_{11}^b & m_{12}^b & 0 & m_{13}^b & m_{14}^b & 0\\ m_{21}^b & m_{22}^b & 0 & m_{23}^b & m_{24}^b & 0\\ 0 & 0 & m_{11}^a & 0 & 0 & m_{12}^a\\ m_{31}^b & m_{32}^b & 0 & m_{33}^b & m_{34}^b & 0\\ m_{41}^b & m_{42}^b & 0 & m_{43}^b & m_{44}^b & 0\\ 0 & 0 & m_{21}^a & 0 & 0 & m_{22}^a\end{bmatrix};\ \left[k_e\right]=\begin{bmatrix}k_{11}^b & k_{12}^b & 0 & k_{13}^b & k_{14}^b & 0\\ k_{21}^b & k_{22}^b & 0 & k_{23}^b & k_{24}^b & 0\\ 0 & 0 & k_{11}^a & 0 & 0 & k_{12}^a\\ k_{31}^b & k_{32}^b & 0 & k_{33}^b & k_{34}^b & 0\\ k_{41}^b & k_{42}^b & 0 & k_{43}^b & k_{44}^b & 0\\ 0 & 0 & k_{21}^a & 0 & 0 & k_{22}^a\end{bmatrix}, \tag{3}$$

where a_{ij} defines (i, j) th element of matrix [a].

To ensure that the compatibility conditions are satisfied at the columns and top beams connections, the transformation of element matrices to a global coordinate system is necessary before the assembly is constructed. In the case of planar structures, all local systems have an axis parallel to an axis of the global system. Fig. 2 shows the case in which the axis u_2 of an arbitrary local system is parallel to the axis U_2 of the global system. For a frame element oriented at an angle from the positive U_3 axis in the clockwise direction, the displacements in global coordinates are given in Equation (4) and Fig. 3.

$$\{u\}=[\Delta]\{U\}. \tag{4}$$

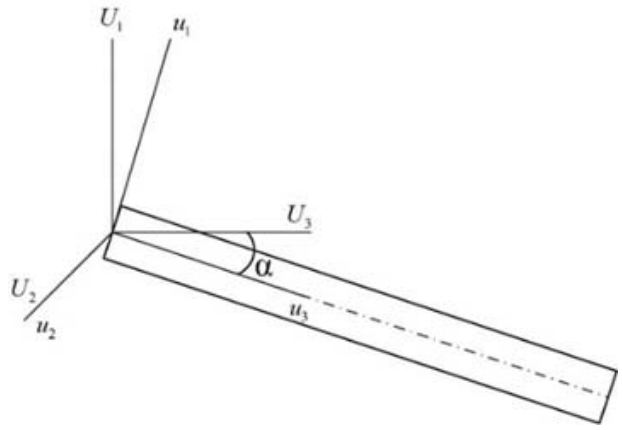

Fig. 3. $u_1 u_2 u_3$: Local coordinate system, $U_1 U_2 U_3$: Global coordinate system.

For the element matrices

$$[\Delta] = \begin{bmatrix} [\Delta_1] & [0] \\ [0] & [\Delta_1] \end{bmatrix}, \tag{5}$$

where

$$[\Delta_1] = \begin{bmatrix} \cos\alpha & 0 & -\sin\alpha \\ 0 & 1 & 0 \\ \sin\alpha & 0 & \cos\alpha \end{bmatrix}. \tag{6}$$

The element mass and stiffness matrices referred to as the global coordinates are then given by

$$[M_e] = [\Delta]^T [m_e][\Delta]; \quad [K_e] = [\Delta]^T [k_e][\Delta]. \tag{7}$$

The mass and stiffness matrices for the entire structure are assembled, then the overall mass and stiffness matrices are obtained as $[M]$ and $[K]$, respectively.

2.1.2. Geometric Stiffness Matrix. The geometric stiffness matrix of an element is given in Ref. [4] and shown in Equation (8).

$$[\mathrm{k}_{ge}] = \begin{bmatrix} 6/5l & 1/10 & 0 & -6/5l & 1/10 & 0 \\ 1/10 & 2l/15 & 0 & -1/10 & -l/30 & 0 \\ 0 & 0 & 0 & 0 & 0 & 0 \\ -6/5l & -1/10 & 0 & 6/5l & -1/10 & 0 \\ 1/10 & -l/30 & 0 & -1/10 & 2l/15 & 0 \\ 0 & 0 & 0 & 0 & 0 & 0 \end{bmatrix}. \tag{8}$$

The geometric stiffness matrix of an element in terms of global coordinates is then computed as in Equation (9).

$$[K_{ge}] = [\Delta]^T [k_{ge}][\Delta]. \tag{9}$$

The global geometric stiffness matrix of the structure is assembled and [Kg] is obtained in this way.

2.1.3. Equation of energy. Energy equations should be expressed for the Euler beam with an element length l. The elastic potential energy U_e is given in Equation (10):

$$U = \frac{1}{2}E\int_0^l I\left(\frac{d^2v}{dx^2}\right)^2 dx + \frac{1}{2}E\int_0^l A\left(\frac{du}{dx}\right)^2 dx. \tag{10}$$

The kinetic energy of the beam element is given in Eq. 11:

$$T = \frac{1}{2}\rho\int_0^l A\left(\frac{dv}{dt}\right)^2 dx + \frac{1}{2}\rho\int_0^l A\left(\frac{du}{dt}\right)^2 dx. \tag{11}$$

2.1.4. Equation of motion. The equation of motion of the undamped system can be expressed using the Lagrange method and energy equations;

$$[M]\{\ddot{q}\} + \left[[K] - P(t)[K_g]\right]\{q\} = \{0\}, \tag{12}$$

where $[M], [K],$ and $[K_g]$ are global mass, elastic stiffness and geometric stiffness matrix, respectively.

The periodic load $P(t) = P_0 + P_t \cos\Omega t$ consists of two parts: P_0 is the static load and P_t is the amplitude of the time-dependent component with frequency Ω. The static and time-dependent components of the load can be represented as a fraction of the fundamental buckling load P_{cr}. Therefore, substituting $P(t) = \alpha P_{cr} + \beta P_{cr}\cos\Omega t$ in Equation (10) gives [13]:

$$[M]\left\{\ddot{q}\right\} + \left[[K] - (\alpha P_{cr} \pm \beta P_{cr}\cos\Omega t)[K_g]\right]\{q\} = \{0\}, \tag{13}$$

where static load parameter $\alpha = P_0/P_{cr}$ and dynamic load parameter is $\beta = P_t/P_{cr}$.

From Equation (11), it can be seen that this equation is a Mathieu-Hill-type linear second order differential equation with a periodic coefficient. According to the theory of linear equations with periodic coefficients, the boundaries between stable and unstable solutions of Equation (11) are formed by periodic solutions of period T and $2T$, where $T = 2\pi/\Omega$. Ref. [1] showed that solutions with a period of 2T are of greater practical importance as the widths of these unstable regions are generally larger than the corresponding solutions with period T. As a first approximation, assume a periodic solution with period 2T. Using this solution along with Equation (11) yields the following equation [12]:

$$\left[[K] - \left(\alpha \pm \frac{1}{2}\beta\right)P_{cr}[K_g] - \frac{\Omega^2}{4}[M]\right]\{q\} = \{0\}. \tag{14}$$

Equation (14) represents the solution of the three related problems:

- Free vibration with $\alpha = 0,\ \beta = 0,$ and the natural frequency $\omega = \Omega/2,$ Equation (15):

$$\left[[K] - \omega^2[M]\right]\{q\} = \{0\}. \tag{15}$$

- Static stability with $\alpha = 1, \beta = 0$ and $\Omega = 0,$ Equation (16):

$$\left[[K] - P_{cr}[K_g]\right]\{q\} = \{0\}. \tag{16}$$

- Dynamic stability when all terms are present, Equation (17):

$$\left[[K] - \left(\alpha \pm \frac{1}{2}\beta\right)P_{cr}[K_g] - \frac{\Omega^2}{4}[M]\right]\{q\} = \{0\}. \tag{17}$$

3. Results.

In this study, the static and dynamic stability of diamond-shaped frames with various boundary conditions (BC) (Fig. 4) and the inclination angle θ under point load applied in vertical direction have been investigated. The beams forming the frame are Euler-Bernoulli beams and have the length of $L_1 = 200$ mm and $L_2 = 0,2L_1$. The material properties of beams are $h = 5$ mm, $h_1 = 0,1h, b = 20$ mm, the mass density $\rho = 7700\ \mathrm{kg/m^3}$, Young's modulus $E = 210$ GPa. The structure consisting of tapered beams has also been discussed and the effect of taper on the instability regions is examined. In addition, the effects of boundary conditions and inclination angle on instability regions have been analyzed. Calculations made in the MATLAB program (present work) are compared with the ANSYS program results for verification.

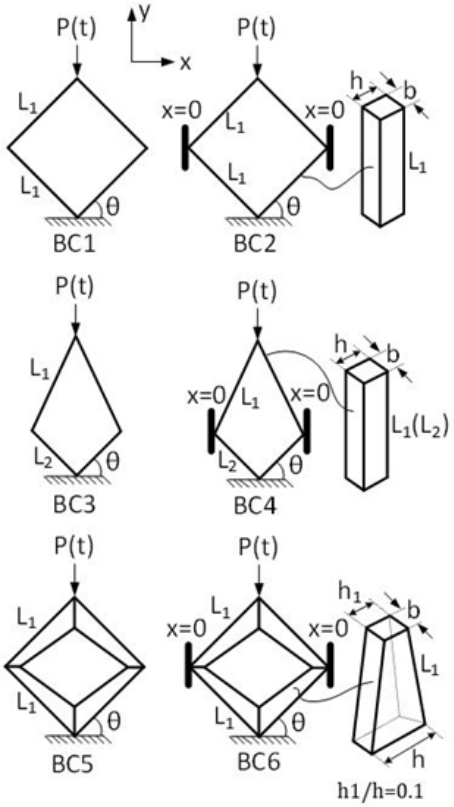

Fig. 4. Boundary conditions.

3.1. Static Stability (Buckling) Analysis. It is expected that the critical buckling load is dependent on the inclination angle θ and different values for the critical buckling load will be obtained if θ is changed. Depending on the variation of the angle θ, shown in Fig. 4, the critical buckling loads of the diamond-shaped beam structure are calculated by using the finite element method and results are given in Table 1. It is clear that the differences in results between the current study and the ANSYS program for frames with different boundary conditions and angle θ are acceptable.

The frame with boundary conditions BC2, BC4 and BC6, which are similar, exhibits the same characteristics depending on θ. Namely, the critical buckling loads have shown a tendency parallel to θ and increased with increasing θ values. Contrary to the previous case, for the boundary conditions of BC1, BC3 and BC5, increased θ values caused a reduction in critical buckling loads.

Table 1. Variations of the critical buckling load values with angle θ and boundary conditions are shown in Fig. 4.

	P_{cr}(N)								
	BC 1			BC 2			BC 3		
θ	Ansys	Present work	Eror (%)	Ansys	Present work	Eror (%)	Ansys	Present work	Eror (%)
15°	13224	13240,243	0,123	7280,6	7233,745	0,648	3416,1	3324,7800	2,7466
30°	6846,3	6852,833	0,095	13972	13977,501	0,039	2931,8	2915,4700	0,5601
45°	4840,8	4852,7099	0,245	19734	19769,902	0,182	2589,1	2582,0294	0,2738
60^0	3951,3	3954,7391	0,087	24157	24221,410	0,266	2364,3	2363,0220	0,0541
75^0	3535,9	3545,8675	0,281	26931	27014,477	0,309	2231,9	2236,1074	0,1882
	P_{cr}(N)								
	BC 4			BC 5			BC 6		
θ	Ansys	Present work	Eror (%)	Ansys	Present work	Eror (%)	Ansys	Present work	Eror (%)
15^0	7007,5	7007,1951	0,004	2256	2228,3566	1,241	342,99	329,1570	4,203
30^0	7749,1	7755,2572	0,079	1168,9	1153,3898	1,345	661,52	635,9800	4,016
45^0	8168,9	8176,4459	0,092	826,72	816,8347	1,210	935,22	899,5500	3,965
60^0	8506,3	8513,1412	0,080	675,04	665,8850	1,375	1145,3	1254,3974	8,697
75^0	8725,6	8734,9750	0,107	605,08	598,0000	1,184	1277,3	1230,0000	3,846

3.2. Natural Frequency. The natural frequencies are given in Table 2 for different boundary conditions. For BC2, BC4 and BC6, the frames have the same character. On the other hand for BC1, BC3 and BC5, if the angle θ increases, the frequency values also decrease. This means that an increase in θ values makes the structure more flexible.

3.3. Dynamic Stability Analysis. Due to having the greatest practical importance, the principal instability region close to $\Omega = 2\omega$ are studied for the boundary conditions given in Fig. 4. Here, Ω and ω are forcing frequency and the first natural frequency which is given in Table 2, respectively. Analyzes are performed for the different values of the following parameters:

1) θ angle $(\theta = 15, 30, 45, 60, 75)$;

2) length ratio of beams ($L_1/L_2 = 0,5$ and 1);

3) static load parameter $\alpha(\alpha = 0$ and $0,5)$;

4) dynamic load parameter β (β is from 0 to 1 and β is from 0 to 2). When the static load parameter is 0, the dynamic load parameter is from 0 to 2, and, when the static load parameter is 0,5, the dynamic load parameter is from 0 to 1.

Table 2. The first natural frequency (Hz).

θ	BC 1	BC 2	BC 3	BC 4	BC 5	BC 6
15^0	66,364	342,98	26,086	98,012	33,133	129,365
30^0	53,277	344,867	22,65	98,08	36,76	129,422
45^0	43,579	344,807	20,16	98,02	29,076	129,39
60^0	37,742	343,724	18,51	97,80	24,23	129,274
75^0	34,677	337	17,56	96,59	21,9	128,59

When the static load parameter $\alpha = 0,5$ and the dynamic load parameter β varies in the range [0, 1], unstable regions become narrower as θ increases as shown in Fig. 5.

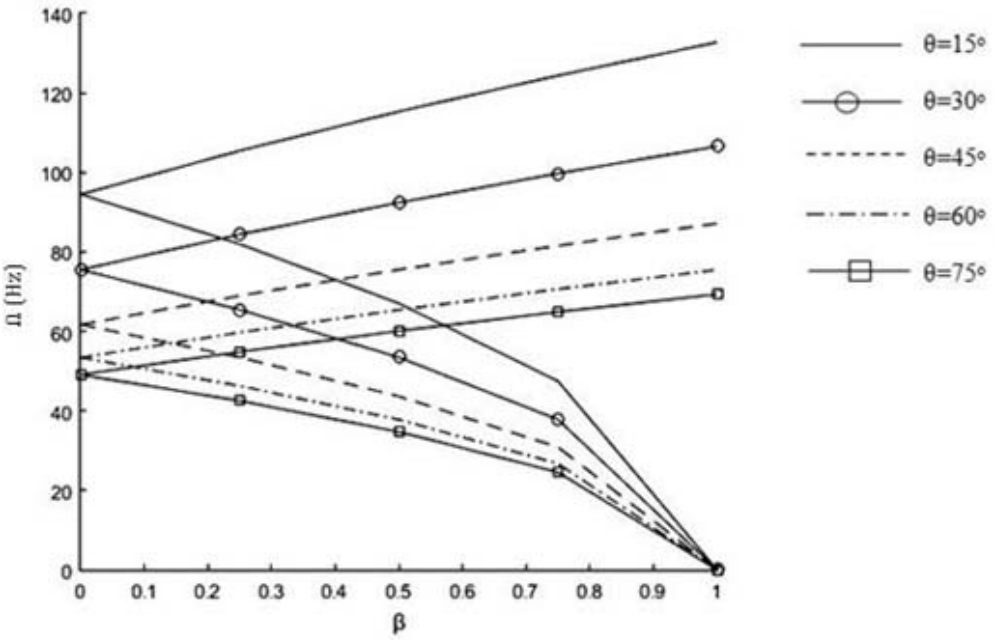

Fig. 5. Effect of $\alpha = 0,5$ on the first dynamic instability regions of BC1.

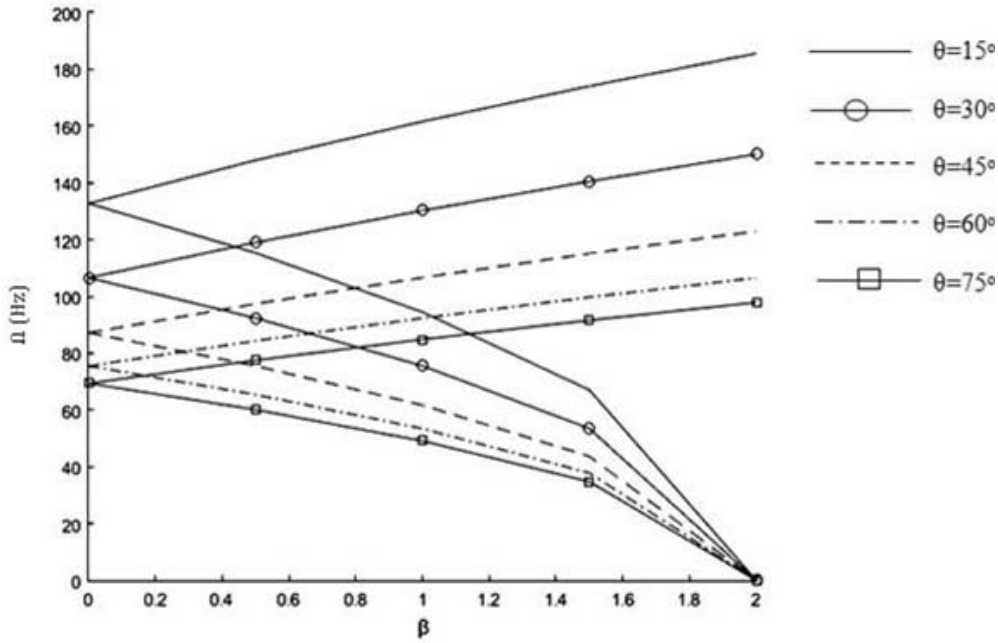

Fig. 6. Effect of $\alpha = 0$ on the first dynamic instability regions of BC1.

In Fig. 6, the static load parameter α is taken as zero and the dynamic load parameter β varies in the range [0, 2]. In comparison with Fig. 5, forcing frequencies increase but

similar behavior for unstable regions for the same θ values has been observed. When the dynamic load parameter $\beta = 0$ and the static load parameter $\alpha = 0,$ it is seen that the graph shifts upward.

For the structure having boundary condition BC2 shown in Fig. 4, an increase in θ angle causes a slight change in the unstable regions as seen in Fig. 7 and Fig. 8.

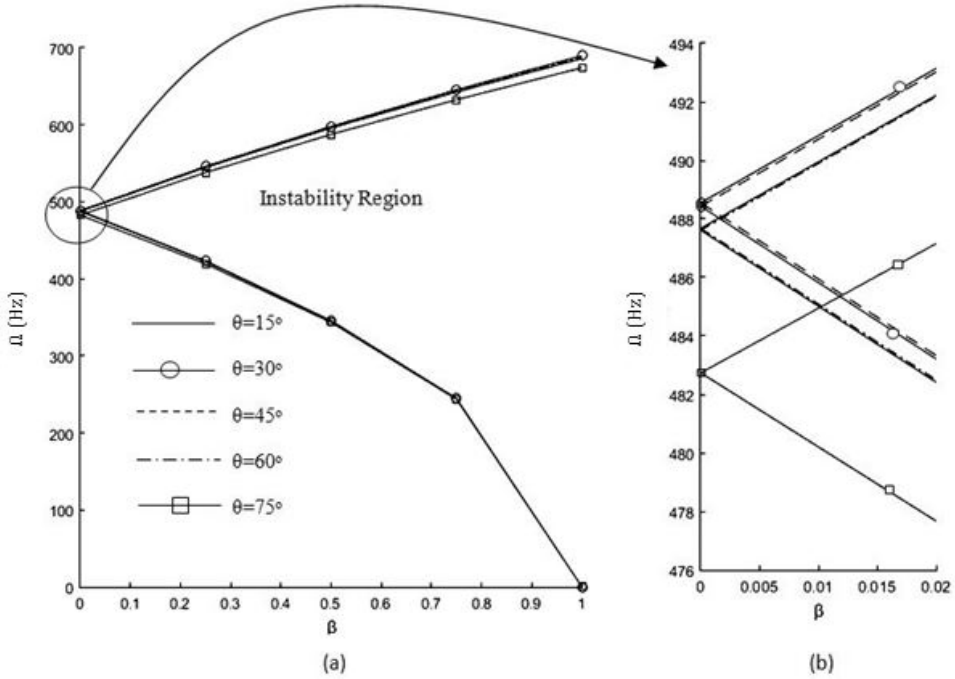

Fig. 7. Effect of $\alpha = 0,5$ on the first dynamic instability regions of BC2.

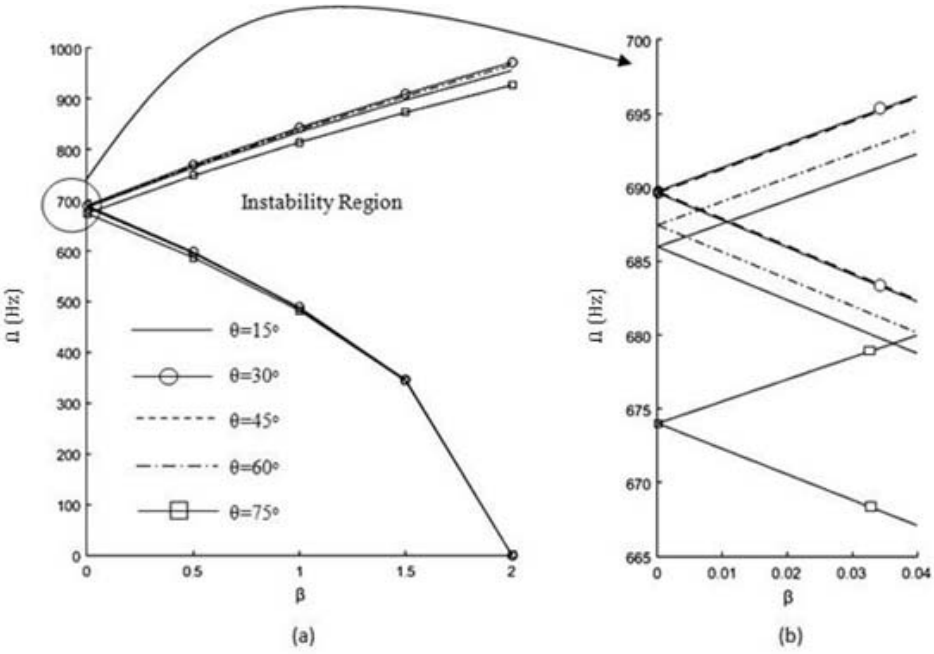

Fig. 8 Effect of $\alpha = 0$ on the first dynamic instability regions of BC2.

Fig. 9 and Fig. 10 are plotted for the structure given in Fig. 4 for the boundary condition of BC3. Fig. 9 and Fig. 10 show that the frequencies of applied loads slightly increase when the static load parameter α decreases.

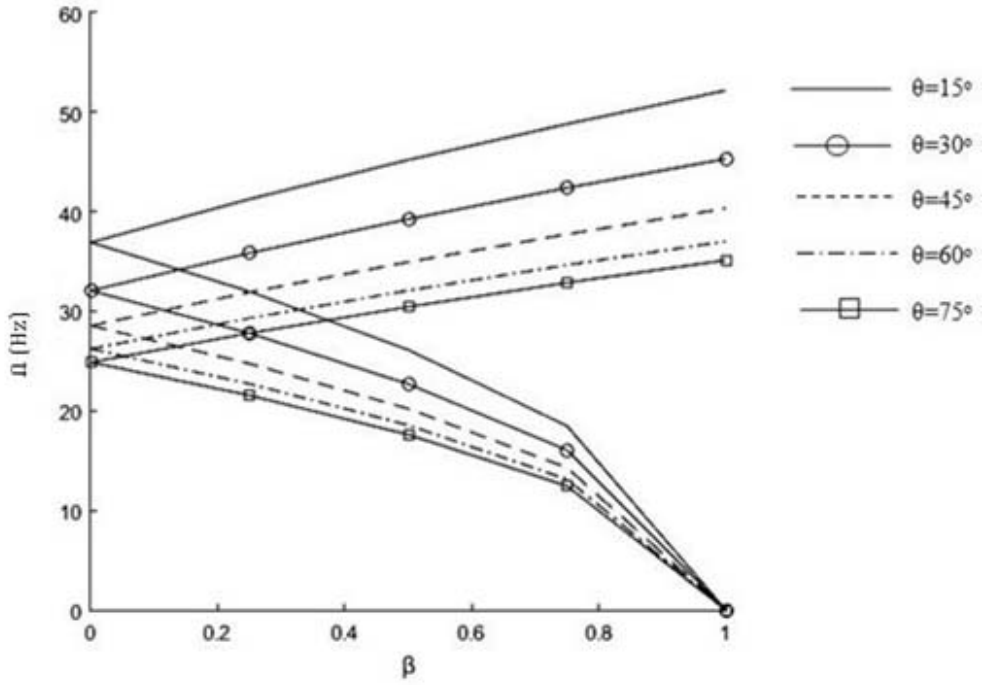

Fig. 9. Effect of $\alpha = 0,5$ on the first dynamic instability regions of BC3.

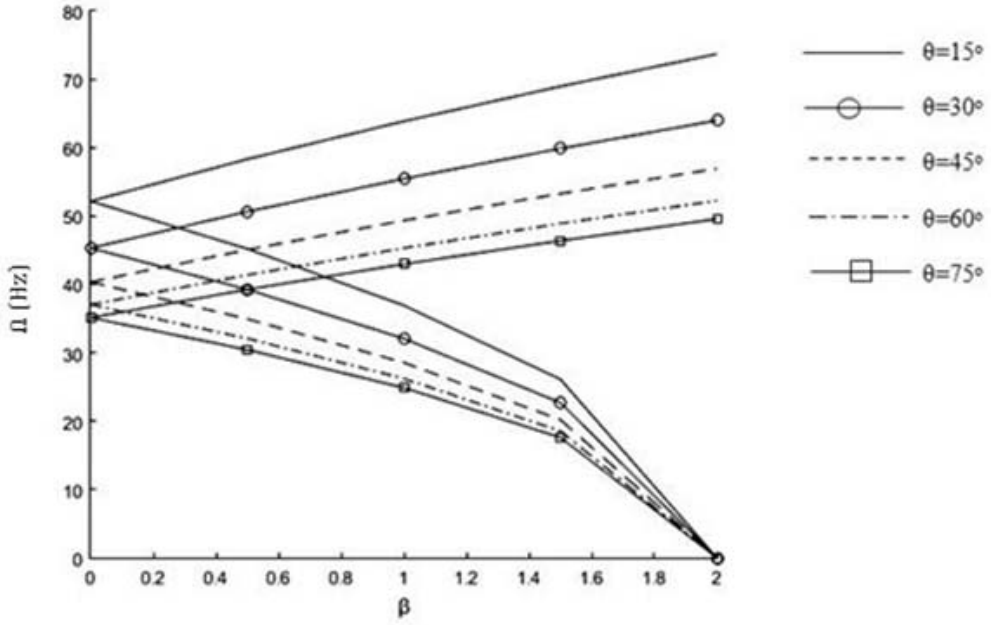

Fig. 10. Effect of $\alpha = 0$ on the first dynamic instability regions of BC3.

The regions of instability for the static load parameter value of $\alpha = 0,5$ and $\alpha = 0$ are shown in Fig. 11 and Fig. 12 for the boundary condition BC4. As seen in Fig. 11 and Fig. 12 an increase in θ angle causes a slight change in the unstable region. It is observed from these graphs that the widths of unstable regions are not changed by θ values.

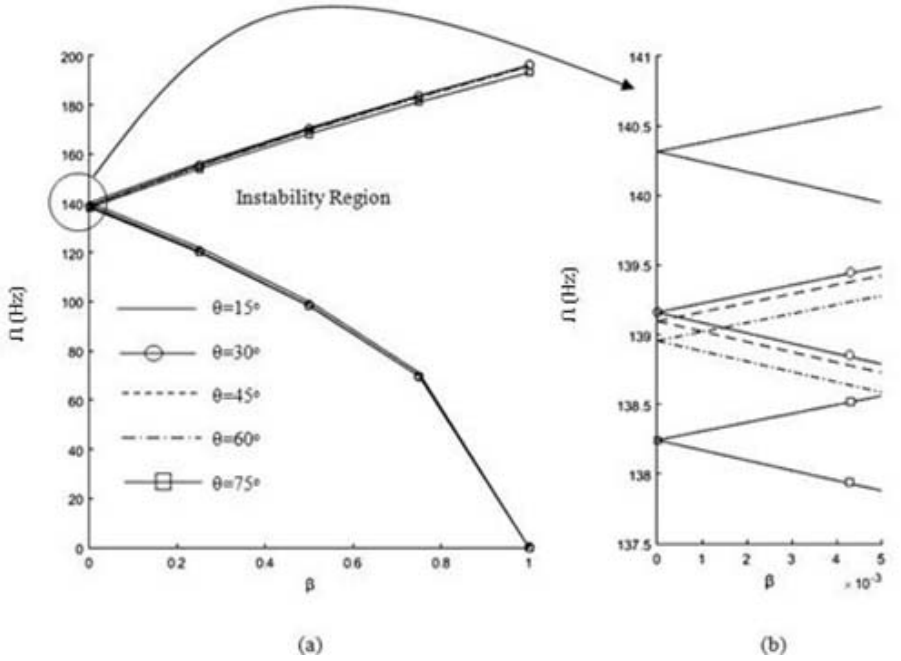

Fig. 11. Effect of $\alpha = 0,5$ on the first dynamic instability regions of BC4.

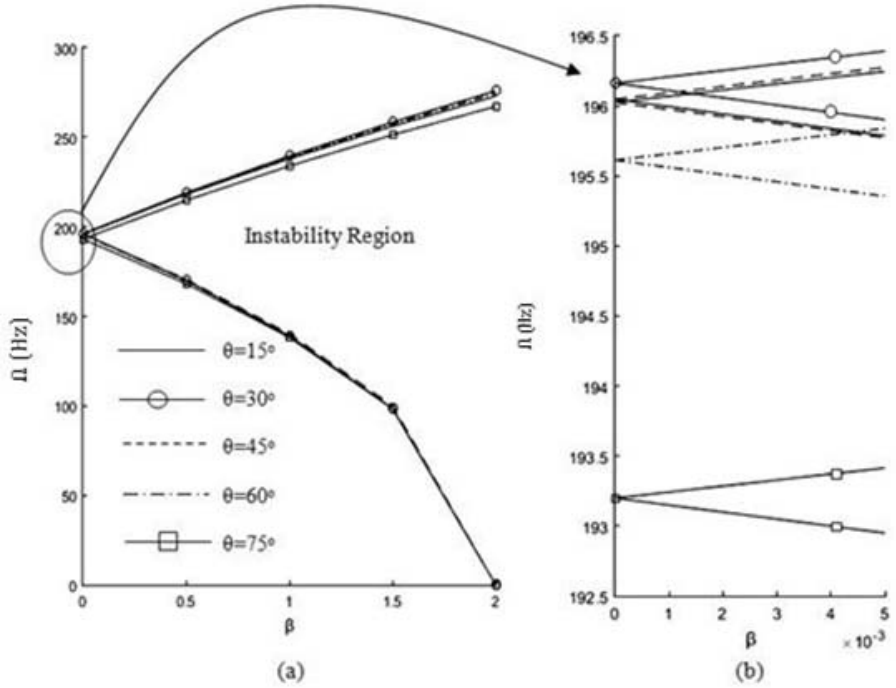

Fig. 12. Effect of C on the first dynamic instability regions of BC4.

Fig. 13 and Fig. 14 show the regions of instability for boundary condition BC5 with the static load parameter $\alpha = 0,5$ and $\alpha = 0$ for various θ values. It is determined that as the static load parameter increases the regions of instability shift downward. Moreover, it is observed that the effect of θ on the unstable dynamic region of BC5 is more than the other diamond- shaped frames.

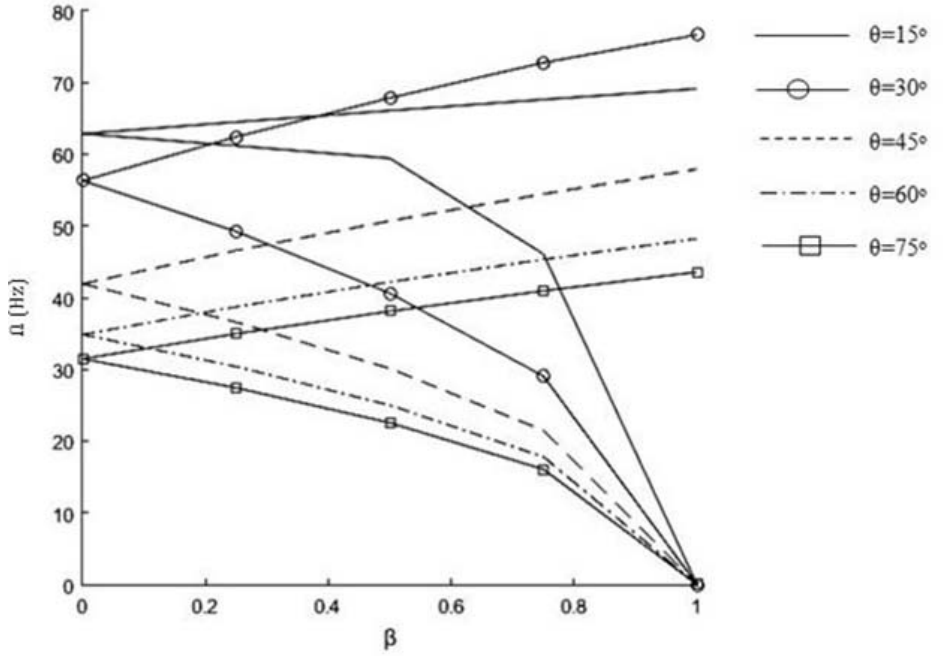

Fig. 13. Effect of $\alpha = 0,5$ on the first dynamic instability regions of BC5.

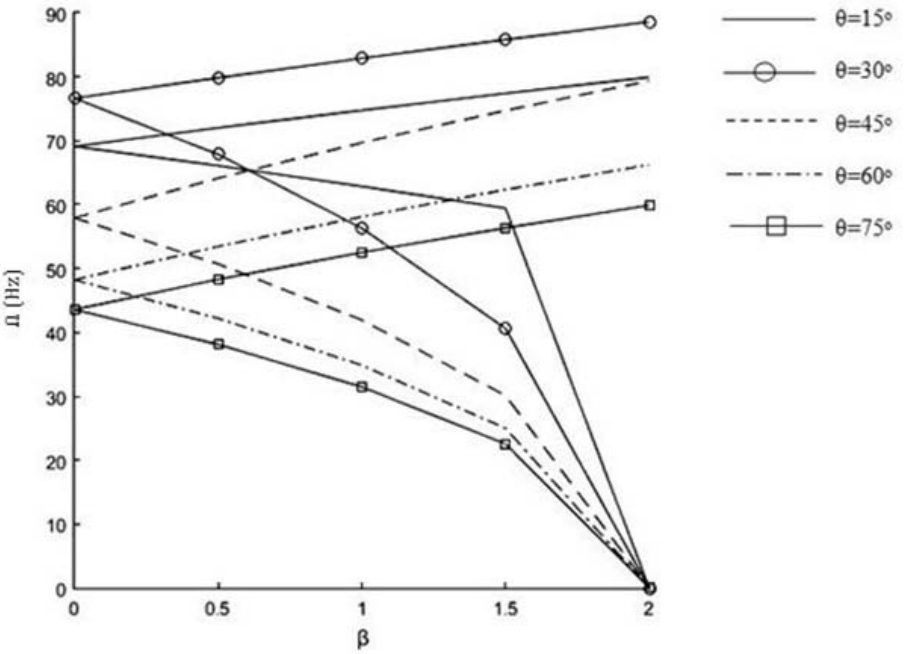

Fig. 14. Effect of $\alpha = 0$ on the first dynamic instability regions of BC5.

Fig. 15 and Fig. 16 are plotted for the structure given in Fig. 4 for BC6. If the static load parameter $\alpha = 0,$ the frequencies of applied force decrease with an increasing angle. This situation is also the same when the static load parameter $\alpha = 0,5.$ However, the static load parameter $a = 0,5$ has smaller frequency values than the static load parameter $a = 0.$ Unstable regions exhibit a negligible change in both cases as shown in Fig. 15 and Fig. 16

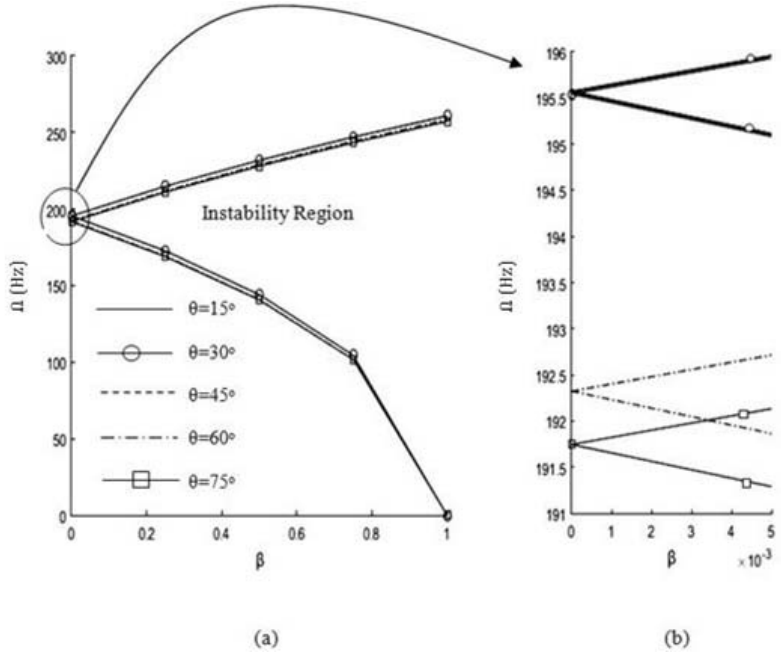

Fig. 15. Effect of $\alpha = 0,5$ on the first dynamic instability regions of BC6.

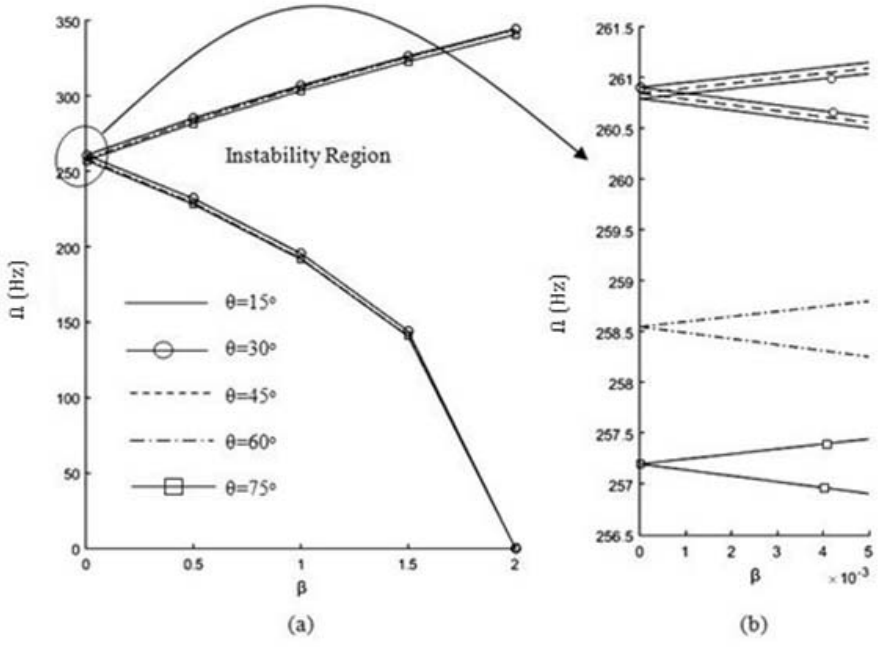

Fig. 16. Effect of $\alpha = 0$ on the first dynamic instability regions of BC6.

4. Discussion and Conclusion.

In this study, the effect of various boundary conditions on the dynamic stability of diamond- shaped frames has been studied. The instability regions are determined for various boundary conditions, inclination angles, beam lengths, taper ratio and static load parameters. Conclusions drawn from the current analysis are that:

(1) In boundary conditions where displacement in the horizontal direction is zero, the effect of θ on the instability regions is negligible.

(2) When the angle θ increases, natural frequencies decrease. If the beam has a tapered cross-section, as the beam length increases, beams become more flexible and the natural frequencies decrease.

(3) If the angle θ and beam length increase and the beam has a tapered cross-section, the critical buckling load decreases for BC1, BC3, and BC5.

(4) The effect of θ angle on the frequencies is negligible for all diamond-shaped frame structures having BC2, BC4 and BC6. This is perhaps due to the rigidity of the system. On the other hand if θ increases, the critical buckling load also increases for these boundary conditions.

(5) By changing the static and dynamic load parameters, length of beam and type of cross-section of beam for different boundary conditions, the dynamic stability regions of the diamond frame structures show variable values.

(6) The regions of instability are the widest when inclination angle θ takes the value $15°$ for a frame consisting of a uniform beam. As the θ value increases, the instability regions become narrower.

(7) For the case of the tapered beam, the instability regions are widest at $\theta = 30°$ and become the narrowest at $\theta = 15°$.

Acknowledgment: Professor M. SABUNCU passed away on May 8, 2018. We would like to thank him for his support, effort, and guidance throughout this study.

Declarations.

- The authors have no conflicts of interest to declare that are relevant to the content of this article.
- The authors have no financial or proprietary interests in any material discussed in this article.

РЕЗЮМЕ. Досліджено динамічну та статичну стійкість ромбоподібних балкових конструкцій під дією періодичного навантаження. Припущено, що структура ромбоподібної форми є балкою Ейлера та моделюється за допомогою методу скінченних елементів. Використано підхід Болотіна для знаходження областей динамічної нестійкості. Власні частоти та навантаження втрати стійкості, отримані зі згенерованої програми скінченних елементів, порівнюються з результатами програми ANSYS. Крім того, досліджено вплив різних граничних умов, кутів нахилу, довжини балки, балки з конічним поперечним перерізом і параметрів статичного/динамічного навантаження на області нестійкості.

КЛЮЧОВІ СЛОВА: ромбоподібна рама, динамічна стійкість, скінченний елемент, статичні та динамічні навантаження.

References.

1. *Bolotin V.V.* (1964), Dynamic Stability of Elastic Systems, San Francisco, Holden Day.
2. *Park S.K., Gao X-L.* (2006), ‘’Bernoulli-Euler beam model based on a modified couple stress theory.’’, J. Micromech. Microeng, 16, 2355 – 2359.

3. *Falsone G., Settineri, D.* (2011), ‘’Euler-Bernoulli-like finite element method for Timoshenko beams.’’, Mech. Res. Commun, 38, 12 – 16.
4. *Briseghella L., Majorana C.E., Pellegrino C.* (1998), ‘’Dynamic stability of elastic structures: A finite element approach.’’, Comput. Struct, 69, 11 – 25.
5. *Girgin K., Özmen G., Orakdöğen E.* (2006), ‘’Buckling lengths of irregular frame columns.’’, J. Constr. Steel Res, 62, 605 – 613.
6. *Zaslavsky A.* (1981), ‘’Stability of portal frames with hinged girders under a moving load.’’ Eng. Struct, 3(2), 96 – 104.
7. *Thomas J., Belek H.T.* (1977), ‘’Free vibration of blade packets.’’, J. Mech. Eng. Science, 19, 13-21.
8. *Lin H.P., Ro J.* (2003) ‘’Vibration analysis of planar serial-frame structures.’’, J. Sound Vib., 262, 1113 – 1131.
9. *Kawashima S.* (1984), ‘’Vibration analysis of frames with semi-rigid connections.’’, Comput. Struct 1984, 19, 85 – 92.
10. *Öztürk H., Yeşilyurt İ., Sabuncu M.* (2006), ‘’In-plane stability analysis of non-uniform cross-sectioned curved beams.’’, J. Sound Vib., 296, 277 – 291
11. *Karaağaç C., Öztürk H., Sabuncu M.* (2011), ‘’ Crack effects on the in-plane static and dynamic stabilities of a curved beam with an edge crack.’’, J. Sound Vib., 330, 1718 – 1736.
12. *Öztürk H., Sabuncu M.* (2005), ‘’Stability analysis of a cantilever composite beam on elestic supports.’’, Compos. Sci. and Technol. 65, 1982 – 1995.
13. *Öztürk H., Yashar A., Sabuncu M.* (2015), ‘’Dynamic stability of cracked multi-span frame structures.’’, Mech. Adv. Mater. Struct., 23, 715 – 726.
14. *İbrahim A.M., Öztürk H., Sabuncu M.* (2012), ‘’Vibration analysis of cracked frame structures.’’ Struct. Eng. Mech., 45, 33 – 52.
15. *Lee H.P.* (1995), ‘’Dynamic stability of a tapered cantilever beam an elastic foundation subjected to a follower force.’’ Int. J. Solids Struct., 33, 1409 – 1424.
16. *Covill D., Begg S., Elton E., Milne M., Morris R., Katz T.* (2014), ‘’Parametric finite element analysis of bicycle frame geometries.’’ Procedia Eng., 72, 441 – 446.
17. *Jenkins J.A., Seitz T.B., Przemieniecki J.S.* (1996), ‘’Large deflections of diamond-shaped frames.’’ Int. J. Solids Struct., 2, 591 – 603.

From the Editorial Board: The article corresponds completely to submitted manuscript

Надійшла 16.06.2021 Затверджена до друку 19.07.2022
